HHS Public Access

Author manuscript

IEEE Trans Biomed Eng. Author manuscript; available in PMC 2020 June 01.

Published in final edited form as:

IEEE Trans Biomed Eng. 2019 June ; 66(6): 1705–1713. doi:10.1109/TBME.2018.2878555.

Viscoelastic Properties of Human Autopsy Brain Tissues as Biomarkers for Alzheimer's Diseases

Kihan Park[*] **[Student Member, IEEE]**,
Medical Robotics and Automation Laboratory (RoboMed) in the Wallace H. Coulter Department of Biomedical Engineering, Georgia Institute of Technology, Atlanta, GA, USA.

Gabrielle E. Lonsberry,
Medical Robotics and Automation Laboratory (RoboMed) in the Wallace H. Coulter Department of Biomedical Engineering, Georgia Institute of Technology, Atlanta, GA, USA.

Marla Gearing,
Department of Pathology and Laboratory Medicine, Emory University School of Medicine, Atlanta, GA, USA.

Allan I. Levey, and
Department of Neurology, Emory University School of Medicine, Atlanta, GA, USA.

Jaydev P. Desai [Fellow, IEEE]
Medical Robotics and Automation Laboratory (RoboMed) in the Wallace H. Coulter Department of Biomedical Engineering, Georgia Institute of Technology, Atlanta, GA, USA.

Abstract

Objective: The present study investigates viscoelastic properties of human autopsy brain tissue via nanoindentation to find feasible biomarkers for Alzheimer's Disease (AD) in *ex vivo* condition and to understand the mechanics of the human brain better, especially on the difference before and after progression of AD.

Methods: Viscoelastic properties of paraformaldehyde-fixed, paraffin-embedded thin (8 μm) sectioned normal and AD affected human autopsy brain tissue samples are investigated via nanoindentation with a combined loading profile of a linear preloading and a sinusoidal loading at various loading frequencies from 0.01 - 10 *Hz*. In 1,200 indentation tests for 10 human autopsy brain tissue samples from 10 different subjects (5 AD cases and 5 normal controls), viscoelastic properties such as Young's modulus, storage modulus, loss modulus, and loss factor of both gray and white matter brain tissues samples from normal and AD affected tissues were measured experimentally.

Results: We found that the normal brain tissues have higher Young's modulus values than the AD affected brain tissues by 23.5 % and 27.9 % on average for gray and white matter, respectively, with statistically significant differences ($p < 0.0001$) between the normal and AD affected brain tissues. Additionally, the AD affected brain tissues have much higher loss factor than the normal brain tissues on lower loading frequencies.

[*]correspondence kihan@gatech.edu.

Significance: AD is one of the leading causes of death in America and continues to affect a growing population. The challenges of recognizing the early pathological changes in brain tissue due to AD and diagnosing a patient has led to much research focused on finding biomarkers for the disease. In this regard, understanding the mechanics of brain tissues is increasingly recognized to play an important role in diagnosing brain diseases.

I. Introduction

Alzheimer's Disease (AD) is a progressive, irreversible, degenerative brain disease that affects an individual's memory that is not normalized by cueing [1]. AD continues to grow in significance as the disease affects more individuals. The Alzheimer's Association reports that AD is the sixth leading cause of fatalities in the United States of America and the fifth leading cause of fatalities in individuals 65 years of age and older, while it is estimated that 5.7 million Americans are living with AD in 2018 [2]. Furthermore, every 65 seconds an individual develops AD and by 2050 it is projected that this time will drop to every 33 seconds [2]. The financial effect of the growing impact of AD is also of great concern with the total payments for health care, long-term care, and hospice for people with AD and other dementias are estimated to be $277 billion in the United States in 2018 [2].

With the growing number of people affected by AD diagnosing the disease has quickly become the forefront of much research. However, with the inconstancies in and limitations of AD diagnosis only 1 in about every 4 individuals who have developed the disease are diagnosed and there are currently no treatments or therapies that delay or prevent the onset of AD [2]–[4]. Currently, AD can only be diagnosed unequivocally postmortem through brain tissue examination from an autopsy [2]. Preclinical AD, a stage where AD pathology in the brain takes place but no symptoms are yet apparent in the individual, is predicted to begin up to a decade or longer before any cognitive effects can be detected. It is only after considerable neuron loss in the brain that deterioration can be clinically detected [5]. Thus, AD biomarkers and brain imaging techniques are being explored to detect the onset of AD.

Specific neuropathological changes in AD affected brain tissue include neurofibrillary tangles and extracellular parenchymal lesions [6]. As AD progresses, significant synaptic deterioration resulting in brain atrophy and amyloid protein accumulation is present [7]. According to current studies, AD affects grey and white matter of brain tissue differently. One study presents the notion that white matter hyperintensities' volume levels are elevated in individuals that have AD and can be present years before the onset of symptoms [8]. Along with the integrity of white matter being compromised in the corpus callosum, the hippocampal volume also diminishes [9]. Another study shows that grey matter atrophy occurs in the left parahippocampal gyrus, left posterior cingulate gyrus, right fusiform gyrus and right superior frontal gyrus [10]. Analyzing these specific structures of the brain are bringing about novel ways to identify, classify, and interpret different stages of AD. Furthermore, investigating the mechanical properties of AD affected brain tissue can bring about new approaches to detect AD. For example, many research groups investigated the mechanical properties of amyloid-β (Aβ) (1-40) amyloid fibril which is one of the well-known biomarkers for AD and reported its Young's modulus as 2-31 GPa under various loading conditions [11]–[13].

Indentation is widely used for mechanical characterization of biological soft tissues, since it is currently the most accessible way to quantitatively measure mechanical properties of a sample [14]–[17]. Many research groups, including ourselves, have investigated the characterization of biological materials such as soft tissues and cells via indentation and the results have shown that it can be used for finding a biomarker indicating the onset of certain diseases [16]–[24]. Since load-displacement curves from an indentation test do not directly yield material properties, additional analysis efforts such as transferring the experimental results to stress-strain curves are required. Unlike a tensile or a compression test, however, transferring load-displacement curves to stress-strain curves is another challenging problem in indentation for accurate characterization of material properties [25]. For example, there are many different definitions of the contact areas depending on the geometry of tips and indentation strain to obtain stress-strain curves from indentation and they yield inconsistent results each other [26]–[29]. Although the accuracy of stress-strain curves from indentation has been improved significantly by combining numerical techniques such as finite element methods, a standardized method to obtain stress-strain curves from indentation for accurate characterization of viscoelastic soft materials has not yet been established [30].

In this paper, we aim to investigate viscoelastic properties of human autopsy brain tissues via nanoindentation to find a feasible biomarker for AD. In section II, modeling for viscoelastic materials, preparation of human autopsy brain tissue samples, and experimental setup are described, while the experimental results with discussion and the concluding remarks are in sections III and IV, respectively.

II. Materials and Methods

A. Human Autopsy Brain Tissue Preparation

Human autopsy brain tissues were carefully selected from archival tissue resources at Neuropathology Core, Emory Alzheimer's Disease Research Center. The human autopsy brain tissues used for the experiment were all sampled from frontal lobes of 10 subjects (5 subjects diagnosed with AD and 5 normal control subjects). Paraformaldehyde-fixed, paraffin-embedded tissue blocks were sliced at 8 μm thick and sections were mounted on standard glass slides. To ensure the sample preparation conditions were constant in terms of microtome thickness setting and environmental conditions, all specimens in this experiment were sliced and transferred in the same setup.

It is known that there is a significant loss of proteins on a human autopsy brain tissue sample within 22 or more hours of the postmortem interval (PMI) [31]. The loss of proteins may cause morphological modification of the tissue accompanied with changes in mechanical properties. Therefore, all samples used for the experiments were screened so that every sample had less than 15 hours of PMI. Since a study reports that mechanical properties of brain tissues vary with the age of the subject [32]–[35], only subjects with ages ranging from 60-75 years for both AD and control group were selected. The details about the human autopsy brain tissue samples used for the experiment can be found in Table I.

The sections were deparaffinized immediately before the indentation experiment according to the protocol: 3 changes of xylene - 5 minutes each followed by acetone, 100% EtOH,

95% EtOH - about 1 min each, then rinse in phosphate-buffered saline (PBS) (1-2 times) and immersed in PBS holding solution until the experiment.

B. Nanoindentation with Circular Flat-ended Tip for Viscoelastic Materials

Nanoindentation experiments have been performed with various tip geometries such as spheres, pyramids, cylindrical flat punches, cones, and wedges. It is difficult to conclude that a certain type of tip geometry provides the best solution for viscoelastic characterization since each geometry has its unique advantages and disadvantages. The cylindrical flat punch and the circular flat-ended tip geometry not only keep the contact area consistent throughout the indentation without being affected by transient behavior or thermal drift but also mitigate a severe problem of sharp tips with finding the contact point accurately [36]. According to the theoretical model of flat punch indenter for a semi-infinite plane surface, the applied axial load to the sample, P, is given by [37], [38]:

$$P = \frac{2ERd}{(1 - v^2)} \quad (1)$$

where, E is the Young's modulus of the sample, R is the radius of the circular flat-ended tip, d is the indentation depth, and v is the Poisson's ratio of the sample. This model assumes frictionless contact with zero contact angle between the indenter and the sample. The theoretical model assumes an ideal contact between the sample and the indenter without interaction between a sample and cylindrical wall. Under this assumption, the theoretical model can be applied to any circular flat-ended indenter tip as well.

By choosing a circular flat-ended tip, stress and strain are only proportional to load and indentation depth, respectively. This makes the constitutive analysis much easier, especially in dynamic loading conditions since the excitation loading frequency and the resultant frequency of stress are the same similar to a simple tensile or compression test.

The load profile consists of a linear pre-loading, one full cycle of sinusoidal loading, and unloading as shown in Fig. 1(a). Generally, a dynamic loading test utilizes a sinusoidal loading profile due to the ease of analysis for both tensile and compressive phase at a single test. Since indentation only includes a compressive phase, the linear pre-loading phase is added before the sinusoidal loading phase as an offset so that the full sinusoidal loading can be performed while the indenter and the sample are being engaged. From the measurement of load-indentation depth at the pre-loading phase, Young's modulus of the sample, E, is obtained (see Fig. 1(b). Then, the sinusoidal loading phase can be analyzed in the stress-strain domain similar to a general dynamic loading test via parallel translation as shown in Fig. 1(c).

When a sinusoidally varying stress is applied to a viscoelastic material, the resulting strain eventually reaches a sinusoidal steady state having the same frequency but delayed in phase [39]. The strain lags the stress and it is true regardless which parameter, either the strain or the stress, is the controlled variable [39]. Since the actual stress applied to the sample is

proportional to the loading, the stress and the strain in the sinusoidal loading phase can be described as:

$$\sigma_{dy}^{*} = \sigma_0 e^{i\frac{2\pi}{T}t} \quad (2)$$

$$\varepsilon_{dy}^{*} = \varepsilon_0 e^{i\frac{2\pi}{T}t} \quad (3)$$

where, the asterisk denotes a complex quantity, σ_0 is the amplitude of the stress, ε_0 is the amplitude of the strain, $i = \sqrt{-1}$, t is the time elapsed from the initiation of a sinusoidal loading ($0 \leq t \leq T$), and T is the period of a sinusoidal loading.

It is useful to express the stress as a complex quantity that consists of the real part in phase with the strain and the imaginary part a quarter cycle out of phase with the strain, while the real and imaginary parts represent elastic stress component and dissipative stress component, respectively. This algebraic maneuver is widely used for the analysis of harmonic systems such as reactive electrical circuits. The complex stress can be formulated as [39]:

$$\sigma_{dy}^{*} = \sigma_e + i\,\sigma_d = (E' + i\,E'')\varepsilon_{dy}^{*} = E'(1 + i\,\eta)\varepsilon_{dy}^{*} \quad (4)$$

where, σ_e is the elastic stress component, σ_d is the dissipative stress component, E' is the storage modulus, E'' is the loss modulus, and η is the loss factor of a viscoelastic material. By the definition, viscoelastic properties, the loss factor, η, the storage modulus, E', and the loss modulus, E'', are expressed as:

$$\eta = \frac{\sigma_d}{\sigma_e} = \frac{E''}{E'} = tan\delta > 0 \quad (\because 0 < \delta < \frac{\pi}{4}) \quad (5)$$

$$E' = \frac{\sigma_e}{\varepsilon_0} = \frac{\sigma_0\, cos\delta}{\varepsilon_0} \quad (6)$$

$$E'' = \frac{\sigma_d}{\varepsilon_0} = \frac{\sigma_0\, sin\delta}{\varepsilon_0} = \eta E' \quad (7)$$

where δ is the angle in a complex plane of a complex stress (or complex modulus) measured from the real axis. From the relations in Eqn. (5)-(7), once any two out of three viscoelastic

properties, η, E', and E'' are given, the remaining value can be calculated by the other two. However, since the stress-strain curve from a sinusoidal stress loading does not have a closed form, which means σ_0 and ε_0 are not constant during the sinusoidal loading due to the inherent nonlinear responses of biological tissues such as creep and stress relaxation, σ_0 and ε_0 are difficult to be measured accurately from the stress-strain curve directly. Therefore, the viscoelastic properties are estimated by the complex stress-strain model with measurable quantities from the stress-strain curve.

Using Euler's formula, $e^{i\theta} = cos\theta + i\,sin\theta$, Eqn. (4) yields the stress-strain relation during sinusoidal loading and is given by:

$$\begin{aligned}\sigma_{dy} &= \sigma_0 \sin\left(\frac{2\pi}{T}t\right) \\ &= \underbrace{E'\varepsilon_0 \sin\left(\frac{2\pi}{T}t\right)}_{\text{elastic component, } \sigma_e} + \underbrace{\eta E'\varepsilon_0 \cos\left(\frac{2\pi}{T}t\right)}_{\text{dissipative component, } \sigma_d} \\ &= E'\varepsilon_{dy} \pm \eta E'\sqrt{\varepsilon_0^2 - \varepsilon_0^2 \sin^2\left(\frac{2\pi}{T}t\right)} \\ &= E'\varepsilon_{dy} \pm \eta E'\sqrt{\varepsilon_0^2 - \varepsilon_{dy}^2}\end{aligned} \tag{8}$$

where, $\sigma_0 = |\sigma_{dy}^*| = \sqrt{(\sigma_e)^2 + (\sigma_d)^2}$, $\sigma_{dy} = \sigma - \sigma_{pre}$, $\varepsilon_{dy} = \varepsilon - \varepsilon_{pre}$, while σ_{pre} and ε_{pre} are the stress and the strain due to the pre-loading, respectively.

By applying the measured stress and strain to the stress-strain relation at the three points A-C on the Fig. 1(c), where the maximum stress state, the stress-free state, and the strain-free state are located, respectively, three viscoelastic properties, η, E', and E'' can be obtained.

At point A, the maximum stress is attained when:

$$\frac{d\sigma_{dy}}{d\varepsilon_{dy}} = 0 \Big|_{\varepsilon_{dy} = (\varepsilon_{dy})_{\sigma_{max}}} \tag{9}$$

This yields:

$$(\varepsilon_{dy})_{\sigma_{max}} = \frac{\varepsilon_0}{\sqrt{1+\eta^2}} \tag{10}$$

At point B, where $\sigma_{dy} = 0$, the strain in the stress-free state, $(\varepsilon_{dy})_{sf}$ is expressed as:

$$(\varepsilon_{dy})_{sf} = \frac{\varepsilon_0}{\sqrt{1+\eta^2}}\eta \quad (11)$$

Similarly, at point C, where $\varepsilon_{dy} = 0$, the stress in the strain-free state, $(\sigma_{dy})_{sf}$ is expressed as:

$$(\sigma_{dy})_{sf} = -\eta E' \varepsilon_0 \quad (12)$$

Using the three measurable quantities, $(\varepsilon_{dy})_{\sigma_{max}}$, $(\varepsilon_{dy})_{sf}$, and $(\sigma_{dy})_{sf}$ from the stress-strain curve, the loss factor η, the storage modulus, E', and the loss modulus, E'' are obtained as:

$$\eta = \frac{(\varepsilon_{dy})_{sf}}{(\varepsilon_{dy})_{\sigma_{max}}} \quad (13)$$

$$E' = -\frac{(\sigma_{dy})_{sf}}{\eta\,\varepsilon_0} = -\frac{(\sigma_{dy})_{sf}}{(\varepsilon_{dy})_{\sigma_{max}}\,\eta\sqrt{1+\eta^2}} \quad (14)$$

$$E'' = \eta E' = -\frac{(\sigma_{dy})_{sf}}{(\varepsilon_{dy})_{\sigma_{max}}\sqrt{1+\eta^2}} \quad (15)$$

It is important to note that η, E', and E'' are all positive quantities because $(\sigma_{dy})_{sf} < 0$

C. Experimental Setup

Ten target regions each for gray and white matter of the human autopsy brain tissue samples are investigated by nanoindentation with a circular flat-ended tip. Each target region covers an area of 90 $\mu m \times 60\ \mu m$ and has 6 indentation points with different loading frequencies (T = 0.1, 0.5, 1, 10, 30 and 100 seconds) for evaluating loading frequency dependent viscoelastic properties of the sample as shown in Fig. 2(a). The target regions are apart from each other at least 1 mm and distributed evenly throughout the sample while avoiding edges of the sample and gray/white matter boundaries to evaluate the spatial heterogeneity of the sample that may exist. The maximum pre-loading is applied for 3 seconds at the rate of 10 $\mu N/sec$, while the amplitude of the sinusoidal loading is set to 12.5 μN.

Fig. 2(b) shows the nanoindentation experimental setup using a commercially available nanoindentation system (TriboIndenter, Hysitron, USA), while a schematic of the contact between the circular flat-ended tip and the sample is shown in Fig. 2(c). By adjusting the load levels carefully, the maximum indentation depth does not exceed 2 % of the sample

thickness in order not to be affected by the glass substrate. We assume that the human brain autopsy tissues are incompressible materials, which yields $v = 0.5$, and each target region of 90 $\mu m \times 60$ μm area is locally homogeneous, so the loading frequency is the only control variable while investigating a target region.

Since biological tissues yield unrepeatable stress-strain response even under the same loading condition unless it is preconditioned [40], the initial indentation dataset at an indentation point is used for the analysis. The mechanical properties of biological soft tissues are also dependent on the environmental temperature and humidity [40]. Therefore, the environmental temperature and the relative humidity were controlled during the experiment to 21 ± 2 °C and 48 ± 5 % (RH), respectively.

D. Statistical Analysis

The two-sample t-test is applied to verify a statistically significant difference in measured viscoelastic properties between the normal and AD affected tissues with the cut-off value of $p < 0.01$ using MATLAB R2016b (MathWorks, Natick, MA, USA).

E. Surface Investigation for Human Autopsy Brain Tissues

To visualize a surface of soft biological tissue through a scanning electron microscope (SEM), it is required to be operated at a low operating voltage so that it does not damage the soft biological sample. Using a low voltage operated SEM machine (SU8010, Hitachi, Japan) at an operating voltage of 1 kV allows the observation of the surface of the normal and AD affected brain tissue as shown in Fig 3. Both gray and white matter of the normal brain tissue are porous and the holes in the tissue are evenly distributed throughout the tissue samples. The distribution and size of the holes in the normal brain tissue are indifferentiable between the two types of matter. Compared to the normal brain tissue, the AD affected brain tissue has enlarged holes and an irregular distribution of the holes. The observations are consistent with a neuropathological criterion for AD diagnosis that the AD affected brain tissues are full of plaques and tangles that disrupt the neuropil [41], [42]. For more quantitative surface analysis, surface roughness of the normal and AD affected brain tissue for 20 $\mu m \times 20$ μm area was measured by an atomic force microscope (AFM) system (Dimension 3100, Veeco, USA) at 6 different locations (3 points on white matter and 3 other points on gray matter) for each sample (Fig. 4). The arithmetic averages of the absolute values of the surface height deviations measured from the mean plane (R_a) of the tissue samples were found. The R_a value for the normal brain tissue is measured to be 256 ± 78 nm while R_a value for the AD affected brain tissue is measured to be 367 ± 102 nm. This 43.4 % increase in R_a value on average shows that the AD affected brain tissue has a rougher surface than the normal brain tissue. Additionally, the normal brain tissue height deviations were distributed evenly throughout the scanned area tissue sample whereas the diseased tissue deviations were clustered together and formed not only longer deviations from the mean plane but wider deviations.

III. Results and Discussion

In the nanoindentation experiment for the human autopsy brain tissues, a total of 1,200 indentations were conducted (20 target regions per sample (10 on each gray and white matter) with 6 different loading frequencies per target region for 10 subjects). Fig. 5 shows the stress-strain curves from the nanoindentation experiment at a target region on each gray and white matter of the normal and AD affected brain tissues and two factors are observed in common which are following: 1) at the pre-loading phase, measured stress and strain shows linear relation that helps to obtain Young's modulus of the sample accurately from the slope of the stress-strain curve, 2) the human autopsy brain tissues behave like a stiffer material when a sinusoidal stress with a higher loading frequency is applied, which is one of the well-known characteristics of a soft tissue [36], [40], [43]. However, the AD affected brain tissues show moderate slopes at the pre-loading phase compared to the normal brain tissues as well as larger hysteresis at the sinusoidal loading phase which mean more energy dissipation during the cycle.

As a more quantitative comparison, Young's modulus values obtained from the nanoindentation experiment with the two-sample *t*-test result are visualized in Fig. 6, while Table II includes the goodness of linear fit for the Young's modulus calculation in addition to the measurements. The normal brain tissues have higher Young's modulus values than the AD affected brain tissues by 23.5 % and 27.9 % on average for gray and white matter, respectively, and there are statistically significant differences ($p < 0.0001$) in the Young's modulus between the normal and AD affected brain tissues for both gray and white matter, although their distributions partially overlap within the one standard deviation. The result showing reduced stiffness on the AD affected brain tissues is consistent with an *in vivo* clinical study using the magnetic resonance elastography, though the reported stiffness values are smaller than our results by four orders of magnitude [44].

Figs. 7 (a)-(c) represent the viscoelastic characterization results of the storage modulus, the loss modulus, and the loss factor along the loading frequencies, respectively. The mean and standard deviation values of each point on the plots were calculated with 50 indentation datasets which came from 10 target regions for 5 subjects. Similar to the Young's modulus result, the storage moduli of the normal brain tissues are higher than the AD affected brain tissues both on gray and white matter by 20.7 – 48.0 % and 6.0 – 46.2 % on average, respectively, over the entire loading frequency range. The loss moduli of the normal and AD affected brain tissues which are obtained by the multiplication of the storage moduli by the loss factors seem to be bounded and more overlapped than the storage moduli for both gray and white matter over the entire loading frequency range. In the case of the loss factor, there is a noticeable difference between the normal and AD affected brain tissues both on gray and white matter at the lower loading frequencies, especially lower than 0.05 *Hz.* The AD affected brain tissues exhibit a more viscous response at the lower loading frequencies compared to normal brain tissues. This can also be observed in the stress-strain curve with larger hysteresis for AD affected brain tissues (see Fig. 5). To check the correlation between the results from the normal and AD affected brain tissues, *p*-values from the two-sample *t*-test between the normal and AD affected brain tissues for the viscoelastic properties were calculated and presented in Table III. There are statistically significant differences between

the normal and AD affected brain tissues especially on gray matter at lower loading frequencies. From the results, we can reasonably infer that the extracellular matrix components of brain tissues undergo changes that result in transition of their viscosity and stiffness both for gray and white matter as AD progresses. However, this needs to be verified with further research.

While analyzing the data, we noticed that there are significantly larger standard deviations on Young's modulus and its linear fitting for AD affected brain tissues (see Fig. 6 and Table II), while the standard deviations for the viscoelastic properties of the normal and AD affected brain tissues are similar levels. We supposed that the difference occurs at the initial contact and/or at the pre-loading phase due to the surface conditions and investigated surfaces of the normal and AD affected brain tissue as well. We presume that the rougher surfaces of the AD affected brain tissues due to the disruption of neuropil result in the larger deviations on the measured properties from the nanoindentation experiment.

Even though the nanoindentation system is able to reliably record indentation experimental data to characterize viscoelastic properties of the human autopsy brain tissues, there are four main limitations of our current study: 1) the mechanical properties obtained from *ex vivo* test are not a predictor of *in situ* or *in vivo* experimental results, 2) the nanoindentation experiment that only involves a single-axis loading mode is not sufficient to fully characterize viscoelastic properties of brain tissue due to its inherent structural complexity and heterogeneity, 3) significantly more brain tissue samples needs to be investigated for evaluating clinical effectiveness of the proposed biomarkers for AD diagnosis, and 4) it is difficult to validate the results due to the huge discrepancy among research reports regarding the characterization of soft tissues. A brain tissue characterization study has reported that gray matter is stiffer than white matter by 12 % [45], which is similar with our experimental results, while there are other studies reporting the opposite results that white matter is stiffer than gray matter by 39 % on average [46] or the storage moduli of gray and white matter are indistinguishable [47]. Storage modulus values reported in other studies using fresh human brain tissues vary from less than 1 kPa to hundreds of kPa and they were measured by different methods at different scales [32], [35], [44], [48]–[51]. The two main reasons why the results have a couple of higher orders of magnitude on the moduli than other studies are presumed to be the tissue fixation and dehydration during the preparation process. In general, it is known that fixation hardens tissue for most types of fixatives including formaldehyde used in this study [52], [53] and there is a report that formalin-fixed human tissues are significantly stiffer (up to 100-fold) than fresh tissues [54]. Moreover, moduli of micron-sized biological samples tend to increase up to four orders of magnitude more than millimetersized or larger samples due to dehydration of the samples [55], [56]. Although there is a huge discrepancy in moduli between fixed tissues and fresh tissues, we hypothesize that the differences in viscoelastic properties of normal and AD affected tissues can be also found on fresh brain tissues and/or in a clinical setup and will try to verify the hypothesis by investigating further studies.

IV. Conclusion

The viscoelastic characterization of human autopsy brain tissues via nanoindentation with a circular flat-ended tip was demonstrated along with preliminary experimental results. Although extra experiments with more samples, a more elaborate protocol, and clinical/pathological cross-checks are required to verify its practical effectiveness, our current work shows the feasibility of using the viscoelastic properties as biomarkers for AD diagnosis. Since the results are consistent with clinical studies reporting AD accompanied with brain atrophy and complex microenvironmental changes on brain tissues, viscoelastic characterization of brain tissue is expected to play a role as quantitative evidence of the clinical observations in neuropathology as well as a novel approach to diagnosing AD postmortem. In our future work, we plan to investigate the viscoelastic properties of various types of diseased brain tissue in various environmental conditions using fresh tissues to ensure the effectiveness of our approach. We hopefully envision that analyzing viscoelastic properties can potentially lead to a new approach of looking at AD affected tissues that can move diagnosis from being retrospective to antemortem. Thereafter, clinical studies would be followed for further *in vivo* investigation to confirm whether the distinct viscoelastic properties of AD affected brain tissues can be also consistently captured by currently available brain imaging techniques, such as elastography.

Acknowledgments

This research was supported by the Emory Alzheimer's Disease Research Center (National Institutes of Health grant: P50AG025688) and performed in part at the Georgia Tech Institute for Electronics and Nanotechnology, a member of the National Nanotechnology Coordinated Infrastructure, which is supported by the National Science Foundation (Grant ECCS-1542174). The content is solely the responsibility of the authors and does not necessarily represent the official views of the National Institutes of Health or National Science Foundation.

References

[1]. Dubois B et al., "Advancing Research Diagnostic Criteria for Alzheimer's Disease: The IWG-2 Criteria," Lancet Neurol., vol. 13, no. 6, pp. 614–629, 2014. [PubMed: 24849862]

[2]. Alzheimer's Association, "2018 Alzheimer's Disease Facts and Figures," Alzheimers Dement., vol. 14, no. 3, pp. 367–429, 2018.

[3]. Prince M et al., "World Alzheimer Report 2016 - Improving Healthcare for People Living with Dementia: Coverage, Quality and Costs Now and in the Future." London, UK: Alzheimer's Disease International (ADI), 2016.

[4]. Liu JL et al., "Assessing the Preparedness of the US Health Care System Infrastructure for an Alzheimer's Treatment." RAND Corporation, 2017.

[5]. Fagan AM et al., "Decreased Cerebrospinal Fluid Aβ42 Correlates with Brain Atrophy in Cognitively Normal Elderly," Ann. Neurol, vol. 65, no. 2, pp. 176–183, 2009. [PubMed: 19260027]

[6]. Dubois B et al., "Revising the Definition of Alzheimer's Disease: A New Lexicon," Lancet Neurol., vol. 9, no. 11, pp. 1118–1127, 2010. [PubMed: 20934914]

[7]. Fox NC and Freeborough PA, "Brain Atrophy Progression Measured from Registered Serial MRI: Validation and Application to Alzheimer's Disease," J. Magn. Reson. Imaging, vol. 7, no. 6, pp. 1069–1075, 1997. [PubMed: 9400851]

[8]. Lee S et al., "White Matter Hyperintensities Are a Core Feature of Alzheimer's Disease: Evidence from the Dominantly Inherited Alzheimer Network," Ann. Neurol, vol. 79, no. 6, pp. 929–939, 2016. [PubMed: 27016429]

[9]. Grady C, "The Cognitive Neuroscience of Ageing," Nat. Rev. Neurosci, vol. 13, no. 7, pp. 491–505, 2012. [PubMed: 22714020]

[10]. Wang W-Y et al., "Voxel-based Meta-analysis of Grey matter Changes in Alzheimer's Disease," Transl. Neurodegener, vol. 4, no. 1, p. 6 (9 pp), 2015. [PubMed: 25834730]

[11]. Xu Z et al., "Alzheimer's Aβ(1-40) Amyloid Fibrils Feature Size-Dependent Mechanical Properties," Biophys. J, vol. 98, no. 10, pp. 2053–2062, 2010. [PubMed: 20483312]

[12]. Paparcone R et al., "Atomistic Simulation of Nanomechanical Properties of Alzheimer's Aβ(1–40) Amyloid Fibrils under Compressive and Tensile Loading," J. Biomech, vol. 43, no. 6, pp. 1196–1201, 2010. [PubMed: 20044089]

[13]. Paparcone R and Buehler MJ, "Failure of Aβ(1–40) Amyloid Fibrils under Tensile Loading," Biomaterials, vol. 32, no. 13, pp. 3367–3374, 2011. [PubMed: 21303720]

[14]. Pathak S and Kalidindi SR, "Spherical Nanoindentation Stress–strain Curves," Mater. Sci. Eng. R Rep, vol. 91, pp. 1–36, 2015.

[15]. Roy R and Desai JP, "Determination of Mechanical Properties of Spatially Heterogeneous Breast Tissue Specimens Using Contact Mode Atomic Force Microscopy (AFM)," Ann. Biomed. Eng, vol. 42, no. 9, pp. 1806–1822, 2014. [PubMed: 25015130]

[16]. Pandya HJ et al., "Simultaneous MEMS-based Electro-mechanical Phenotyping of Breast Cancer," Lab Chip, vol. 15, no. 18, pp. 3695–3706, 2015. [PubMed: 26224116]

[17]. Plodinec M et al., "The Nanomechanical Signature of Breast Cancer," Nat. Nanotechnol, vol. 7, no. 11, pp. 757–765, 2012. [PubMed: 23085644]

[18]. Pandya HJ et al., "Towards a Portable Cancer Diagnostic Tool Using a Disposable MEMS-based Biochip," IEEE Trans. Biomed. Eng, vol. 63, no. 7, pp. 1347–1353, 2016. [PubMed: 26930673]

[19]. Di Carlo D, "A Mechanical Biomarker of Cell State in Medicine," J. Lab. Autom, vol. 17, no. 1, pp. 32–42, 2012. [PubMed: 22357606]

[20]. Park K and Desai JP, "Machine Learning Approach for Breast Cancer Localization," in Int. Conf. Manip. Autom. Robot. Small Scale. IEEE, 2017, pp. 154–159.

[21]. Pandya HJ et al., "Design and Fabrication of a Flexible MEMS-based Electro-mechanical Sensor Array for Breast Cancer Diagnosis," J. Micromech Microeng, vol. 25, no. 7, p. 075025 (13 pp), 2015. [PubMed: 26526747]

[22]. Xu W et al., "Cell Stiffness Is a Biomarker of the Metastatic Potential of Ovarian Cancer Cells," PLoS one, vol. 7, no. 10, p. e46609 (12 pp), 2012. [PubMed: 23056368]

[23]. Park K et al., "Electromechanical Coupling Factor of Breast Tissue as a Biomarker for Breast Cancer," IEEE Trans. Biomed. Eng, vol. 65, no. 1, pp. 96–103, 2018. [PubMed: 28436838]

[24]. Li Q et al., "AFM Indentation Study of Breast Cancer Cells," Biochem. Biophys. Res. Commun, vol. 374, no. 4, pp. 609–613, 2008. [PubMed: 18656442]

[25]. Patel DK and Kalidindi SR, "Correlation of Spherical Nanoindentation Stress-strain Curves to Simple Compression Stress-strain Curves for Elastic-plastic Isotropic Materials Using Finite Element Models," Acta Mater, vol. 112, pp. 295–302, 2016.

[26]. Basu S et al., "On the Determination of Spherical Nanoindentation Stress–strain Curves," J. Mater. Res, vol. 21, no. 10, pp. 2628–2637, 2006.

[27]. Field J and Swain M, "A Simple Predictive Model for Spherical Indentation," J. Mater. Res, vol. 8, no. 2, pp. 297–306, 1993.

[28]. Herbert E et al., "On the Measurement of Stress-strain Curves by Spherical Indentation," Thin Solid Films, vol. 398, pp. 331–335, 2001.

[29]. Fischer-Cripps A and Lawn B, "Indentation Stress-strain Curves for Quasi-ductile Ceramics," Acta Mater, vol. 44, no. 2, pp. 519–527, 1996.

[30]. Pierrat B et al., "Indentation of Heterogeneous Soft Tissue: Local Constitutive Parameter Mapping Using an Inverse Method and an Automated Rig," J. Mech. Behav. Biomed. Mater, vol. 78, pp. 515–528, 2018. [PubMed: 28478915]

[31]. Blair JA et al., "Individual Case Analysis of Postmortem Interval Time on Brain Tissue Preservation," PLoS one, vol. 11, no. 3, p. e0151615 (14 pp), 2016. [PubMed: 26982086]

[32]. Chatelin S et al., "Towards Child Versus Adult Brain Mechanical Properties," J. Mech. Behav. Biomed. Mater, vol. 6, pp. 166–173, 2012. [PubMed: 22301186]

[33]. Gur RC et al., “Gender Differences in Age Effect on Brain Atrophy Measured by Magnetic Resonance Imaging,” Proc. Natl. Acad. Sci. U.S.A, vol. 88, no. 7, pp. 2845–2849, 1991. [PubMed: 2011592]

[34]. Gefen A et al., “Age-dependent Changes in Material Properties of the Brain and Braincase of the Rat,” J. Neurotrauma, vol. 20, no. 11, pp. 1163–1177, 2003. [PubMed: 14651804]

[35]. Prange MT and Margulies SS, “Regional, Directional, and Age-dependent Properties of the Brain Undergoing Large Deformation,” J. Biomech. Eng, vol. 124, no. 2, pp. 244–252, 2002. [PubMed: 12002135]

[36]. Herbert E et al., “Measuring the Constitutive Behavior of Viscoelastic Solids in the Time and Frequency Domain Using Flat Punch Nanoin-dentation,” J. Mater. Res, vol. 24, no. 3, pp. 626–637, 2009.

[37]. McKee CT et al., “Indentation Versus Tensile Measurements of Young’s Modulus for Soft Biological Tissues,” Tissue Eng. Part B Rev, vol. 17, no. 3, pp. 155–164, 2011. [PubMed: 21303220]

[38]. Harding J and Sneddon I, “The Elastic Stresses Produced by the Indentation of the Plane Surface of a Semi-infinite Elastic Solid by a Rigid Punch,” vol. 41, no. 1, pp. 16–26, 1945.

[39]. Roylance D, “Engineering Viscoelasticity” Cambridge, MA, USA: Dep. Mater. Sci. Eng.–Mass. Inst. Tech, 2001, vol. 2139, pp. 1–37.

[40]. Fung YC, Biomechanics: Mechanical Properties of Living Tissues. Springer-Verlag, New York, 1993.

[41]. McKee A et al., “Neuritic Pathology and Dementia in Alzheimer’s Disease,” Ann. Neurol, vol. 30, no. 2, pp. 156–165, 1991. [PubMed: 1910274]

[42]. Coyle JT et al., “Alzheimer’s Disease: A Disorder of Cortical Cholinergic Innervation,” Science, vol. 219, no. 4589, pp. 1184–1190, 1983. [PubMed: 6338589]

[43]. Prevost TP et al., “Dynamic Mechanical Response of Brain Tissue in Indentation In Vivo, In Situ and In Vitro,” Acta Biomater, vol. 7, no. 12, pp. 4090–4101, 2011. [PubMed: 21742064]

[44]. Murphy MC et al., “Decreased Brain Stiffness in Alzheimer’s Disease Determined by Magnetic Resonance Elastography,” J. Magn. Reson. Imaging, vol. 34, no. 3, pp. 494–498, 2011. [PubMed: 21751286]

[45]. Green MA et al., “In Vivo Brain Viscoelastic Properties Measured by Magnetic Resonance Elastography,” NMR Biomed, vol. 21, no. 7, pp. 755–764, 2008. [PubMed: 18457350]

[46]. Budday S et al., “Mechanical Properties of Gray and White Matter Brain Tissue by Indentation,” J. Mech. Behav. Biomed. Mater, vol. 46, pp. 318–330, 2015. [PubMed: 25819199]

[47]. Feng Y et al., “Viscoelastic Properties of the Ferret Brain Measured In Vivo at Multiple Frequencies by Magnetic Resonance Elastography,” J. Biomech, vol. 46, no. 5, pp. 863–870, 2013. [PubMed: 23352648]

[48]. Budday S et al., “Mechanical Characterization of Human Brain Tissue,” Acta Biomater, vol. 48, pp. 319–340, 2017. [PubMed: 27989920]

[49]. Jin X et al., “A Comprehensive Experimental Study on Material Properties of Human Brain Tissue,” J. Biomech, vol. 46, no. 16, pp. 2795–2801, 2013. [PubMed: 24112782]

[50]. Franceschini G et al., “Brain Tissue Deforms Similarly to Filled Elastomers and Follows Consolidation Theory,” J. Mech. Phys. Solids, vol. 54, no. 12, pp. 2592–2620, 2006.

[51]. Fallenstein G et al., “Dynamic Mechanical Properties of Human Brain Tissue,” J. Biomech, vol. 2, no. 3, pp. 217–226, 1969. [PubMed: 16335085]

[52]. Eklund A et al., “A Catheter Tactile Sensor for Measuring Hardness of Soft Tissue: Measurement in a Silicone Model and in an In Vitro Human Prostate Model,” Med. Biol. Eng. Comput, vol. 37, no. 5, pp. 618–624, 1999. [PubMed: 10723900]

[53]. Stickland NC, “A Detailed Analysis of the Effects of Various Fixatives on Animal Tissue with Particular Reference to Muscle Tissue,” Stain Technol, vol. 50, no. 4, pp. 255–264, 1975. [PubMed: 810925]

[54]. Ebenstein DM et al., “Nanomechanical Properties of Calcification, Fibrous Tissue, and Hematoma from Atherosclerotic Plaques,” J. Biomed. Mater. Res. A, vol. 91, no. 4, pp. 1028–1037, 2009. [PubMed: 19107789]

[55]. Ebenstein DM and Pruitt LA, “Nanoindentation of Biological Materials,” Nano Today, vol. 1, no. 3, pp. 26–33, 2006.

[56]. Balooch M et al., “Viscoelastic properties of Demineralized Human Dentin Measured in Water with Atomic Force Microscope (AFM)-based Indentation,” J. Biomed. Mater. Res, vol. 40, no. 4, pp. 539–544, 1998. [PubMed: 9599029]

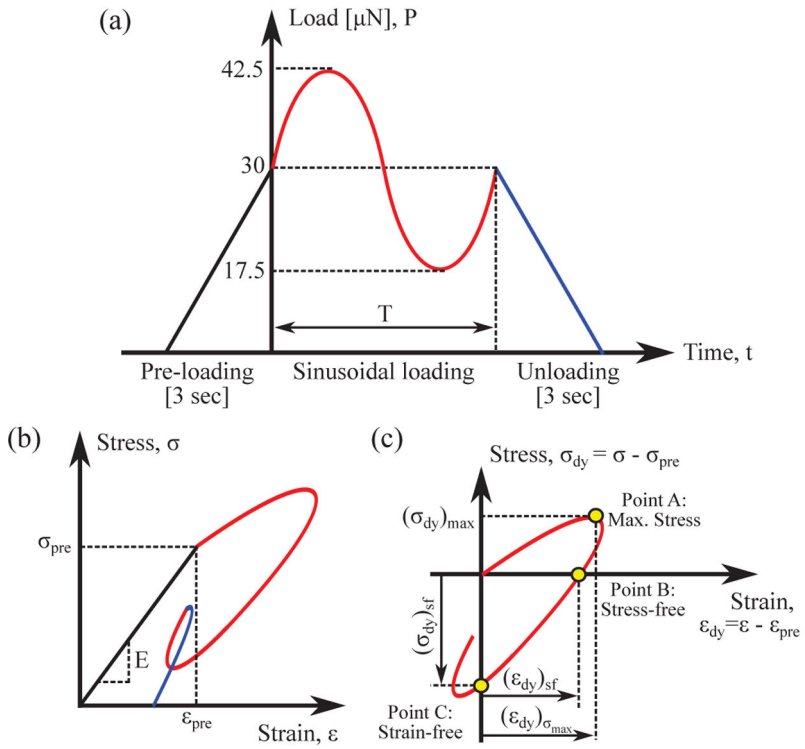

Fig. 1.

(a) Loading profile that consists of pre-loading, sinusoidal loading, and unloading phase, (b) resultant stress-strain curve obtained from the load and indentation depth measurement, and (c) stress-strain curve for the sinusoidal loading phase.

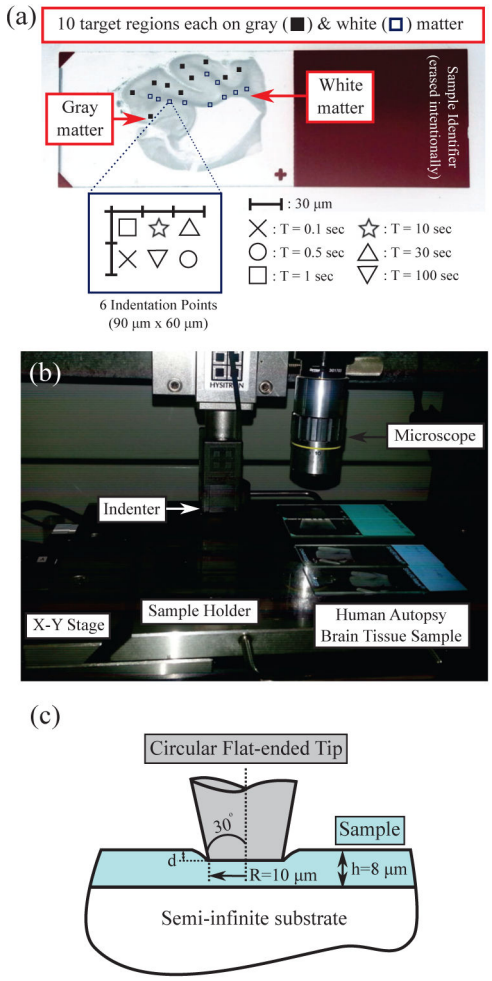

Fig. 2.

Experimental setup for viscoelastic characterization of the human autopsy brain tissue via nanoindentation: (a) brain tissue sample for the experiment, (b) nanoindentation system, and (c) schematic of the contact between the circular flat-ended tip and the sample.

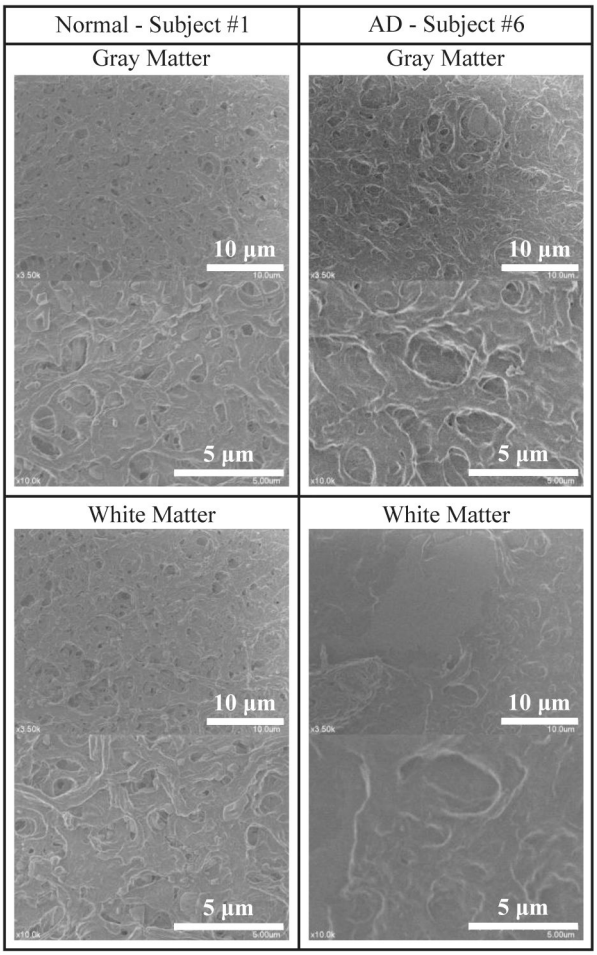

Fig. 3.
Scanning electron microscope (SEM) images of normal and AD affected brain tissue.

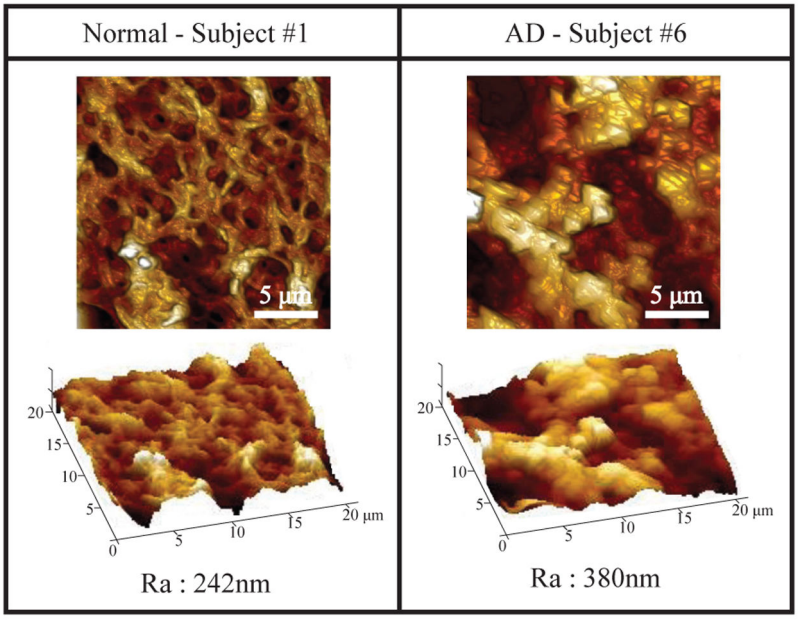

Fig. 4.

Atomic force microscope (AFM) images of normal and AD affected brain tissue with surface roughness, R_a.

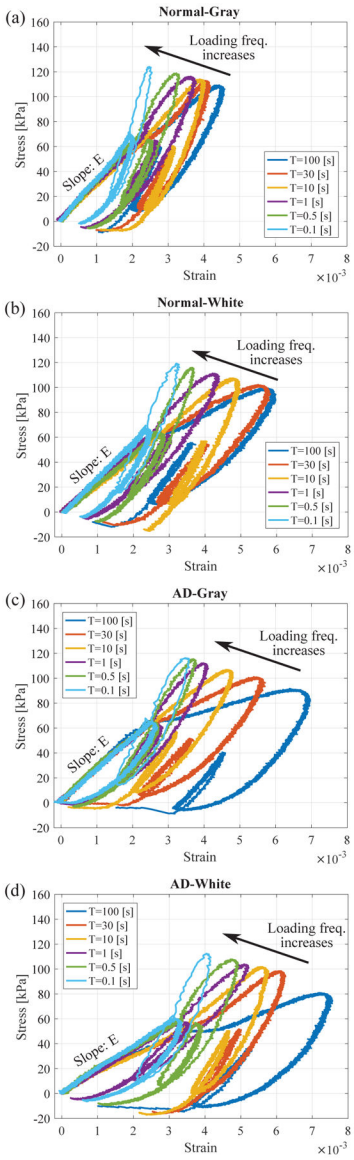

Fig. 5.

Stress-strain curves of human autopsy brain tissues obtained by the nanoindentation experiment: (a) gray matter of normal brain tissue, (b) white matter of normal brain tissue, (c) gray matter of AD affected brain tissue, and (d) white matter of AD affected brain tissue.

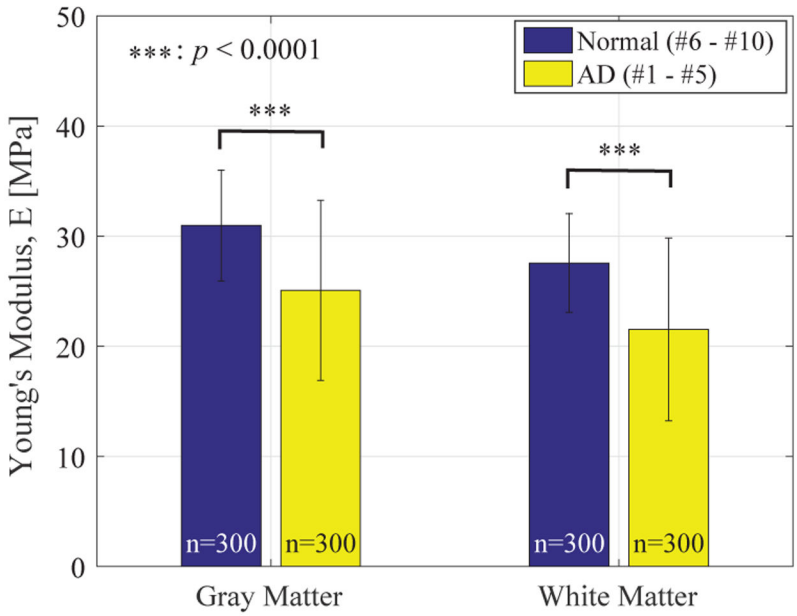

Fig. 6.

Measured Young's modulus, *E,* of normal and AD affected human autopsy brain tissues during the pre-loading phase.

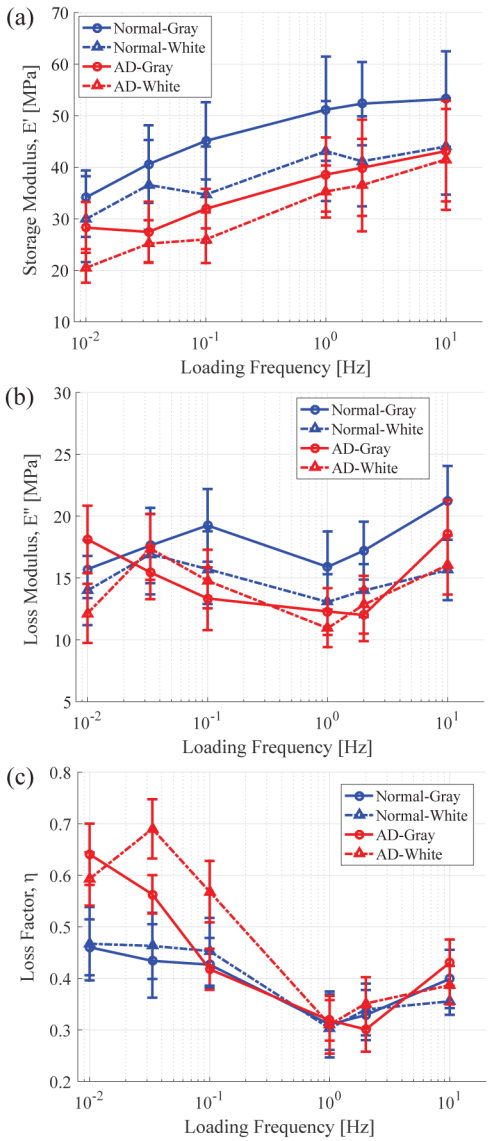

Fig. 7.

Experimental results of viscoelastic characterization for normal and AD affected human autopsy brain tissues: (a) storage modulus, E', (b) loss modulus, E'', and (c) loss factor, η.

TABLE I.

Information for the human autopsy brain tissue samples

Subject #	Diagnosis	PMI (hr)	Age (Onset)	Age (Autopsy)
1	AD	5.5	51	61
2	AD	7	59	72
3	AD	6.5	56	67
4	AD	2.5	60	74
5	AD	14.5	60	68
6	Control	2.5	N/A	70
7	Control	6	N/A	61
8	Control	6	N/A	69
9	Control	11	N/A	68
10	Control	6	N/A	75

PMI: Postmortem interval, AD: Alzheimer’s disease

TABLE II.

Measured Young's modulus of the brain tissue samples

Type	n	E [MPa]	R^2 (Linear fit)
Normal-Gray	300	30.97 ± 5.58	0.987 ± 0.0168
Normal-White		27.54 ± 8.18	0.988 ± 0.0171
AD-Gray		25.08 ± 4.98	0.976 ± 0.0427
AD-White		21.54 ± 8.30	0.969 ± 0.0539

n: the number of indentation datasets

TABLE III

Measured viscoelastic properties of the normal and AD affected brain tissues with *p*-values from the two-sample *t*-test

Type	Loading freq. [Hz]	*n*	E' [MPa]		$p(E')$	E'' [MPa]		$p(E'')$	η		$p(\eta)$
			Normal	AD		Normal	AD		Normal	AD	
Gray matter	0.01	50	34.12 ± 5.31	28.28 ± 4.99	***	15.71 ± 4.95	18.12 ± 5.75	***	0.46 ± 0.05	0.64 ± 0.06	***
	0.033		40.61 ± 7.54	27.45 ± 5.93	***	17.62 ± 6.38	15.45 ± 4.59	***	0.43 ± 0.07	0.56 ± 0.04	***
	0.1		45.11 ± 7.49	31.94 ± 3.96	***	19.24 ± 6.20	13.34 ± 5.34	***	0.42 ±0.05	0.42 ± 0.04	0.51
	1		51.17 ± 9.86	38.58 ± 7.20	***	15.89 ± 6.02	12.29 ± 4.03	***	0.31 ± 0.06	0.32 ± 0.04	0.79
	2		52.33 ± 8.06	39.90 ± 9.28	***	17.20 ± 4.94	12.00 ± 4.49	***	0.33 ± 0.05	0.30 ± 0.04	**
	10		53.23 ± 9.21	43.13 ± 9.69	***	21.23 ± 5.91	18.56 ± 5.79	***	0.40 ± 0.06	0.43 ± 0.05	**
White matter	0.01	50	29.93 ± 8.30	20.47 ± 3.39	***	13.98 ± 5.87	12.14 ± 5.04	**	0.47 ± 0.07	0.59 ± 0.06	***
	0.033		36.57 ± 8.69	25.18 ± 4.24	***	16.93 ± 6.80	17.37 ± 5.59	0.36	0.46 ± 0.06	0.69 ± 0.06	***
	0.1		34.69 ± 9.27	26.00 ± 5.03	***	15.71 ± 6.12	14.77 ± 5.01	0.08	0.45 ± 0.06	0.57 ± 0.06	***
	1		43.13 ± 9.63	35.29 ± 5.13	***	13.06 ± 4.74	10.94 ± 3.31	*	0.30 ± 0.04	0.31 ± 0.05	0.72
	2		41.15 ± 8.69	36.53 ± 8.94	0.01	13.98 ± 4.55	12.83 ± 4.94	0.03	0.34 ± 0.05	0.35 ± 0.05	0.53
	10		44.02 ± 9.28	41.52 ± 9.73	0.37	15.64 ± 5.15	16.05 ± 5.05	0.65	0.36 ± 0.03	0.39 ± 0.04	**

n: the number of pairs of indentation datasets,

*: $p < 0.01$,

**: $p < 0.001$, and

***: $p < 0.0001$

IEEE Trans Biomed Eng. Author manuscript; available in PMC 2020 June 01.